NUMERICAL INVESTIGATION OF THE NORTH WALL PASSIVE THERMAL PERFORMANCE FOR CHINESE SOLAR GREENHOUSE

by

Yiming LI[a], Xingan LIU[b*], Fengsheng QI[c], Li WANG[b], and Tianlai LI[b]

[a]College of Engineering, Shenyang Agricultural University, Shenyang, China
[b]College of Horticulture, Shenyang Agricultural University, Shenyang, China
[c]College of Metallurgy, Northeastern University, Shenyang, China

Original scientific paper
https://doi.org/10.2298/TSCI200229268L

The fully passive solar energy utilization system of Chinese solar greenhouse is efficient for ensuring year-round cultivation of vegetables, owing to the high amount of heat charge and discharge characteristic of the north wall enclosure. In the present research, the thermal performance is investigated using CFD. A 3-D mathematical model has been established to evaluate the wall thickness, layered configuration and material property. The predicted thermal environments are in good agreement with the experimental measurements, indicating the reliability of the established numerical model. The results showed that the increase of north wall thickness could cause the waste of resources due to the thermal masses mainly concentrate in the superficial layer. Constructing layered configuration is recommended for the north wall which uses Styrofoam in the outer layer to reduce heat loss. Nevertheless, the property of north wall material has little effect on the thermal environment. The research results, thus obtained, will give good guidance for completing the Chinese solar greenhouse engineering database and optimizing the solar energy utilization.

Keywords*: greenhouse, solar energy, temperature, north wall*

Introduction

Chinese solar greenhouse (CSG) is an important agricultural facility for sustainable development. It facilitates year-round cultivation of vegetables without any auxiliary heating. Compared with the plastic/glass covered greenhouses as applied in the western countries, the CSG has more reasonable utilizations of renewable energy. It lowers the construction costs in the extreme cold regions. In the CSG, the south roof is covered with plastic film to absorb the energy from solar radiation during the daytime and is replaced with thermal blanket to conserve heat during the night. Nevertheless, the thermal masses are mainly accumulated in the north wall, followed by the soil and the north roof. In northern China, the temperature difference is more than 25 °C between inside and outside of the CSG. The north wall is an essential thermal regenerator in the CSG. The passive solar energy utilization inside the CSG can be

[*]Corresponding author, e-mail: 383666179@qq.com

attributed to the north wall which stores heat in the daytime and releases heat in the night to maintain the suitable microclimate. The enclosure arrangements must be carefully designed when no auxiliary heating is supplied for the winter production of vegetables, fruits and flowers [1-4]. However, most engineers do not have sufficient recognition of the heat transfer mechanism and the internal microclimate optimization. There is a pressing instructional need for the design of thermal enclosures.

The first CSG was designed in Liaoning province in 1930's. With the increasing demand for winter vegetables and the growing maturity of building technology, the CSG rapidly developed in the early 1990's [5]. The Twelfth-six Year Plan (2016-2020) for Chinese Protected Agriculture Development emphasizes that the CSG will continue fast yet steady development focusing on the design pattern and the construction standardization. Statistically, the CSG used in northern China has a large proportion over 80% of the greenhouse areas in China [6]. Several researchers (Bartzanas *et al*. [7], Boulard and Wang [8], Bournet *et al*. [9], Fath and Abdelrahman [10], Kacira *et al.* [11], Mistriotis and Briassoulis [12], Molina-Aiz *et al*. [13], and Vanthoor *et al*. [14]) have successfully studied the thermal environments in the solar greenhouses by employing the numerical simulation. However, their research results as available in the literature could be restricted to the glass greenhouses and plastic greenhouses. In contrast, the CSG has much larger heat masses in the thermal enclosures which make winter production possible by storing and releasing heat in the cold areas.

The early researches (Ajabshirchi *et al*. [15] and Ozturk [16]) were devoted mainly to the experimental part which could visually show the temperature distributions inside the greenhouses. Nevertheless, the repeated measurements are difficult because of the high research costs and long research cycles. So, there existed an urgent need to build a theoretical model to predict the thermal environments of the solar greenhouses. The CFD technique can fill this gap by simulating the time-dependent microclimate inside the solar greenhouses. The CFD methods are equipped to visualize the heat transfer characteristics and temperature distributions in the CSG. Moreover, the numerical simulations are reproducible and unlimited by time and space. The solar energy utilization of the greenhouse has been numerically investigated (Boulard *et al*. [17], Ling *et al*. [18], Tong *et al*. [19], and Zhou *et al*. [20]). Many researchers have testified that the north wall in the CSG is the largest thermal accumulator and the most steerable construction factor. The effect of the north wall configuration on the internal microclimate has been explored by experimental studies and numerical simulations (Ren *et al*. [21], Wang *et al*. [22], and Zhang *et al*. [23]). Nevertheless, the multifarious measurements lack standardization and the results cannot meet the CSG optimization design.

Literatures as reviewed before, mention the needs of further studies to improve the solar energy utilization in greenhouses owing to their important roles of the winter crop cultivation. The CSG design starves for more normalized codes to gain theoretical guidelines for building operations. The numerical simulation needs a more accurate mathematical model to capture the solar radiation and heat transfer details.

In this study, the numerical simulation has been carried out to investigate the microclimate inside the CSG. The effects of wall thickness, layered configuration, and material property have been discussed. The first objective is to develop mathematical modelling to predict the heat transfer details in the CSG. The second objective is to demonstrate the influence of north wall configuration on the microclimate inside the solar greenhouse. And the third objective is to provide theoretical foundation for the construction standardization in the CSG design and optimization.

Experimental set-up

Physical structure of the CSG

In the present study, the numerical investigation and the validated experiment have been carried out in Shenyang (41.8°N, 123.4°E), Liaoning province, the People's Republic of China. The reference CSG in the parameter researches is exhibited in fig. 1. This CSG has 8 m span, 60 m length, and 4 m ridge height. It is facing south and the azimuth is 7° south by west. The architectural structure employs the arched steel truss which eliminates the need of pillars inside the CSG. The south roof is covered by a thin plastic film in the daytime to absorb the solar energy. After that a 0.03 m blanket is placed on it in the night to preserve the heat mass. It is worth mentioning that the blanket is rolled up on the top of the south roof in the daytime, fig. 1(a).

The north roof consists of the back slope and the back roof. It is made of lightweight materials such as wood, mat and the waterproof materials. The north wall is composed of a 0.37 m brick layer inside and a 0.11 m insulation layer outside. It is noteworthy that the north wall has been particularly investigated in this research. The wall thickness, layered configuration and material property are different in the contrasted cases.

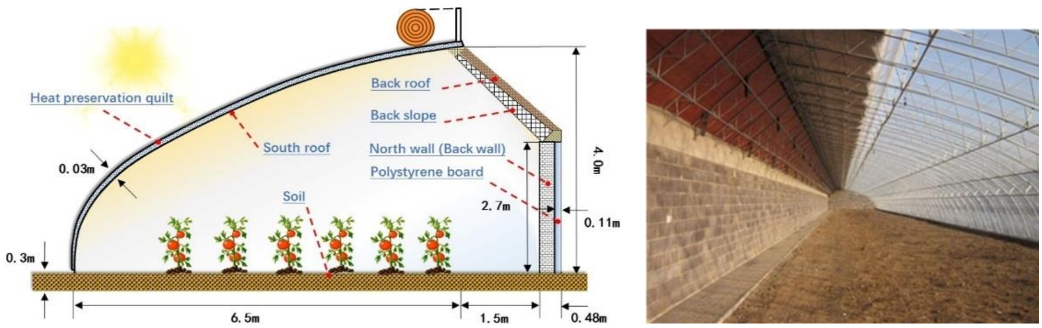

(a) **(b)**

Figure 1. Geometric configuration (a) and internal appearance (b) of the CSG

Experimental measurement

The experimental measurements were conducted in a typical clear day of January 23, 2017. The CSG cases were managed in the same way (*i.e.* 8:30 a. m., rolling up the blanket; 16:00 p. m., rolling down the blanket). The thermal environments inside the CSG have been detected for 24 consecutive hours to obtain an integrated evolution cycle in an entire day. The temperature measurements were carried out at every 10 minutes and the time interval for data processing was 1 hour. The main instrument for measuring the temperature distributions is the *T*-type thermocouple. This temperature sensor has the advantages of high measurement accuracy, short response time, high mechanical strength and good pressure resistance (measuring range –20 °C to 70 °C, resolution: 0.1 °C accuracy at ±0.2%). Moreover, the data are acquired using the CR1000 and CR3000 data collectors produced by Campbell.

There are 14×6 measuring points distributed in the CSG and three thermocouples are used for each measuring point. The multiple temperature sensors are evenly placed inside the greenhouse, inside the soil, on the soil surface and on the north wall surface. And the calculated average values and distribution results serve as the bases for verifying the numerical simulations.

Model establishment

Considering the compressibility of the gas inside the CSG, the gas-flow is identified as the Newtonian fluid which is in accordance with ideal gas conditions. Based on the Reynolds time-average method, the computational domain is iteratively solved. The specific expression of the continuity equation for 3-D unsteady compressible flow is:

$$\frac{\partial \rho}{\partial t}+\frac{\partial(\rho u_i)}{\partial x_i}=0 \tag{1}$$

where ρ is the density, t – the time, and u_i – the velocity components along the x_i.

The expression of the momentum equation is:

$$\frac{\partial(\rho u_i)}{\partial t}+\frac{\partial(\rho u_i u_j)}{\partial x_j}=-\frac{\partial P}{\partial x_i}+\frac{\partial}{\partial x_j}\left[\mu\left(\frac{\partial u_i}{\partial x_j}+\frac{\partial u_j}{\partial x_i}-\frac{2}{3}\delta_{ij}\frac{\partial u_i}{\partial x_j}\right)\right]+\frac{\partial}{\partial x_j}\left(-\rho\overline{u'_i u'_j}\right) \tag{2}$$

This equation must be closed by introducing a model approximation. The Boussinesq hypothesis has been used to relate the Reynolds stress to the average velocity gradient. It can be written:

$$-\rho\overline{u'_i u'_j}=\mu_\mathrm{t}\left(\frac{\partial u_i}{\partial x_j}+\frac{\partial u_j}{\partial x_i}\right)-\frac{2}{3}\left(\rho k+\mu_\mathrm{t}\frac{\partial u_i}{\partial x_i}\right)\delta_{ij} \tag{3}$$

where $-\rho\overline{u'_i u'_j}$ is the Reynolds stress, μ_t is the turbulent viscosity.

The energy equation can be expressed:

$$\frac{\partial}{\partial t}(\rho E)+\frac{\partial}{\partial x_i}[\mu_i(\rho E+P)]=\frac{\partial}{\partial x_j}\left[\left(k+\frac{C\mu_t}{\mathrm{Pr}_t}\right)\frac{\partial T}{\partial x_j}+\mu_i(\tau_{ij})_\mathrm{eff}\right] \tag{4}$$

where E is the total energy and $(\tau_{ij})_\mathrm{eff}$ – the deviatoric stress tensor.

The realizable k-ε turbulence model has significant advantages in predicting the gas-flow and the near-wall flow. Therefore, the present study employed this model in the numerical simulations. The governing equations consist of two transport equations:

$$\frac{\partial}{\partial t}(\rho k)+\frac{\partial}{\partial x_j}(\rho k u_j)=\frac{\partial}{\partial x_j}\left[\left(\mu+\frac{\mu_t}{\sigma_k}\right)\frac{\partial k}{\partial x_j}\right]+G_k+G_b-\rho\varepsilon-Y_m+S_k \tag{5}$$

$$\frac{\partial}{\partial t}(\rho\varepsilon)+\frac{\partial}{\partial x_j}(\rho\varepsilon u_j)=\frac{\partial}{\partial x_j}\left[\left(\mu+\frac{\mu_t}{\sigma_\varepsilon}\right)\frac{\partial\varepsilon}{\partial x_j}\right]+\rho C_1 S_\varepsilon-\rho C_2\frac{\varepsilon^2}{k+\sqrt{v\varepsilon}}+C_{1\varepsilon}\frac{\varepsilon}{k}C_{3\varepsilon}G_b+S_\varepsilon \tag{6}$$

where G_k and G_b represent the generation of turbulence kinetic energy, Y_m – the contribution of the fluctuating dilatation in compressible turbulence to overall dissipation rate, σ_k and σ_ε – the turbulent Prandtl numbers for k and ε, respectively, and S_k and S_ε – the further generation terms.

Meanwhile, the 3-D solar load model is established. This equation is based on a ray tracing algorithm to simulate the dynamic changes of solar radiation. It can be expressed:

$$\frac{\mathrm{d}I(\vec{\mathrm{r}},\vec{\mathrm{s}})}{\mathrm{d}s}+(a+\sigma_s)I(\vec{\mathrm{r}},\vec{\mathrm{s}})=an^2\frac{\sigma T^4}{\pi}+\frac{\sigma_s}{4\pi}\int_0^{4\pi}I(\vec{\mathrm{r}},\vec{\mathrm{s}}')\Phi(\vec{\mathrm{s}},\vec{\mathrm{s}}')\mathrm{d}\Omega' \tag{7}$$

where $\vec{r}$ is the position vector, $\vec{s}$ – the direction vector, σ – the scattering coefficient, a – the absorption coefficient, n – the refractive index, Φ – the phase function, and Ω' – the solid angle.

In order to control the radiation update frequency during continuous phase solution proceeds, model orientation, sunshine factor, geographical location and time zone are imported to the model.

Geometric construction and grid arrangement

The model building is based on the actual configuration of the CSG. Moreover, the construction and material parameters agree with the experimental arrangement. Figure 2(a) displays the geometric construction of the reference case in the parameter research. One should recognize that the soil is identified as 2.2 m deep with a temperature boundary condition in accordance with the experimental measurements. The grid model of the reference case is shown in fig. 2(b). The computational domain is divided into a series of hexahedron elements. Moreover, a refined mesh has been used in local region to improve the prediction precision. The total number of the grids is up to 2.38 million. This grid arrangement has been applied to the other models in the parameter research. And they vary from 1.72 to 2.87 million.

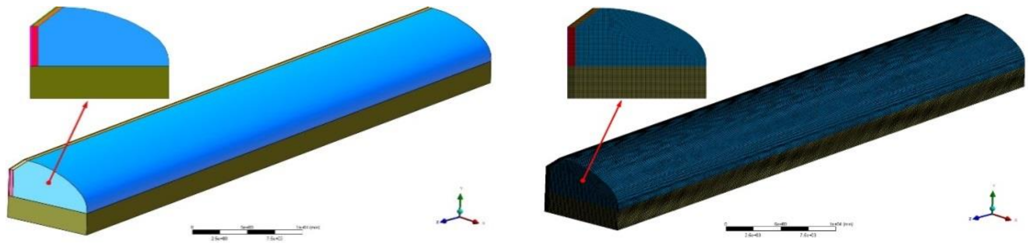

(a) (b)

Figure 2. The 3-D geometrical model (a) and grid arrangement (b) of the CSG

Numerical details

The ANSYS FLUENT 19.0 has been employed in the present research. The numerical simulation is proposed with the finite volume method to spatially discrete the computational domain. Considering the accuracy, stability and economy of the numerical simulation, the pressure solver-based coupling algorithm is adopted for the CSG. The second-order upwind scheme is used for spatial dispersion. The velocity-pressure modification of the air-flow is based on the Coupled algorithm, which has a higher computational precision. The spatial interpolation of the solution domain adopts the quadratic upwind interpolation of convective kinematics (QUICK) scheme, which can effectively avoid numerical oscillations. For the processing of dissipative terms, the second-order central difference format is employed. In order to reduce the computational cost, the standard wall function method is used to satisfy the requirements of the viscous boundary-layer grid in the near-wall region. The numerical simulation is iterated and stored for every time step. The convergence criteria are defined: the residual value of the continuity equation, energy equation and other equations are less than or equal to 10^{-6}, 10^{-8}, and 10^{-4}, respectively. The time step of the numerical simulation is specified as 1 minute and the total calculation time is 24 hours. The governing equations have been solved repeatedly for the whole day cycles and the operating conditions at the end of the time step. These were identified as the initial conditions to restart the calculation until the predicted temperature distributions varied by less than 0.01 °C between cycles.

Result and discussions

Experimental validation

The reference case in the numerical investigation is employed for the experimental validation to verify the feasibility of the CFD approach. Figure 3 demonstrates the temporal evolutions of the gas temperatures and the north wall surface temperatures compared with the experimental measurements in a clear day. The predicted numerical temperatures agree well with the experimental measurements.

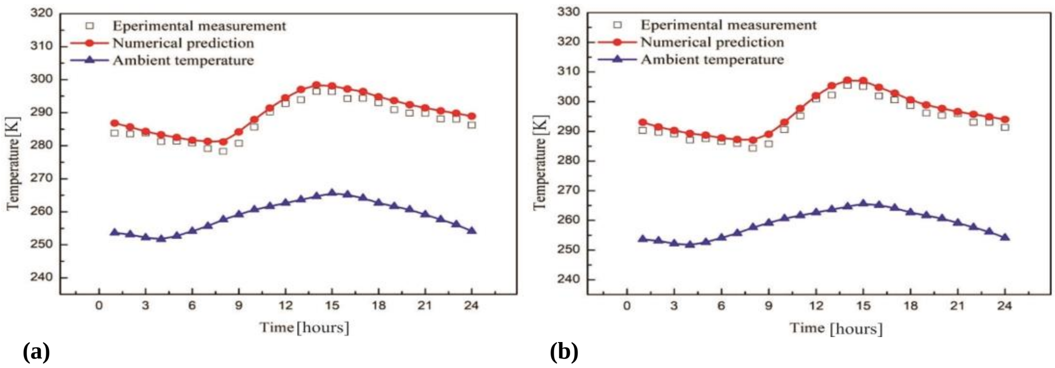

Figure 3. Numerical validations of the air temperature (a) and the north wall surface temperature (b) in comparison to the experimental measurements

The distribution trends are basically the same and the averaged deviation is approximated to 7.3%. The experiments were carried out with many uncertainties such as environmental conditions, instrument precisions and operating errors. In contrast, the numerical predictions were obtained under ideal conditions. The infiltration energy was neglected. And the heat transfers in the soil were insufficient due to the limited computational domain. As a result, the numerical predictions are higher than the experimental data. As can be noticed, the variations of internal temperature and external temperature are out of sync. As the sun rises, the external ambient temperature gradually increases. But the solar energy does not affect the internal environment until the blanket is rolled up at 8:30 a. m. When the solar radiation transmits through the plastic film, the internal gas temperature shows a rapid increase. The peak of the internal gas temperature displays somewhat advanced in contrast to the ambient temperature, while the peak of the wall surface temperature is hysteretic. It is because the internal thermal environment does not depend on the ambient temperature but depends on the solar energy utilization. With the increase of internal energy, the heat fluxes tend to store into the thermal enclosures. The thermal energy conversion results in the advancement of gas temperature peak and the retardation of the wall temperature peak. Both of the numerical simulation and the experimental measurement have successfully captured this peak shifting phenomenon. Since the obtained results of numerical simulation correspond to the experimental measurements, an appropriate method has been established for further parameter research.

Effects of the north wall thickness

In this section, three north wall thicknesses of 170, 370, and 570 mm are investigated to find out the optimal thickness configuration of the north wall in CSG. The primary concern is the gas temperatures inside the CSG during the cold winter. The internal air temperature variations onto different north wall thickness have been shown in fig. 4(a). In general, the gas temperature increases with the increase in the wall thickness. The difference of temperature increase between 170 and 370 mm thickness is significant. But between 370 and 570 mm it is less significant. Thus it is indicated that there is a limit with the north wall thickness. The abusive increase of which could bring about the waste of resources. What needs clarification is that the abrupt decrease in the gas temperature distribution at 4:00 p. m. is caused by the covering change on the south roof. The surface temperatures of north wall under different north wall thickness are shown in fig. 4(b). When the wall thickness is too small, the heat storage of the north wall in the daytime is insufficient. The north wall enclosure releases less heat in the night, and there is not enough heat to keep a suitable thermal environment for crop growth. On the contrary, too thick walls could not contribute much to the temperature improvement. When the wall heat storage reaches optimum, the effect of the wall thickness increase considering thermal performance, is negligible. As a consequence, the design of north wall thickness should be appropriate according to the thermal characteristics of the solar greenhouse environment.

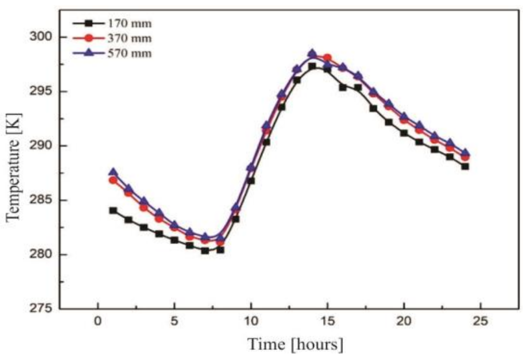

(a)

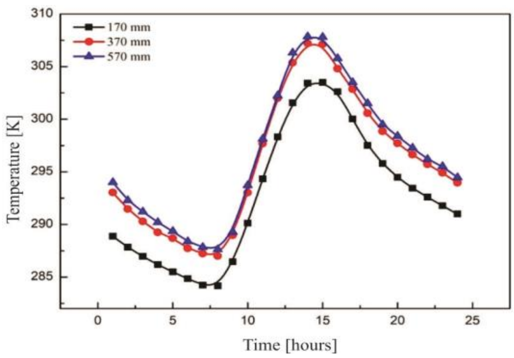

(b)

Figure 4. Effect of north wall thickness on the internal air temperature (a) and north wall temperature (b)

The temperature distributions at three representative cross sections of time (*i. e.* 7:00 a. m., 14:00 p. m. and 12:00 p. m.) throughout a day are illustrated in fig. 5. The temperature contours vividly reflect the heat distribution in the north wall. Due to the heat insulation of the Styrofoam in the outer layer, the heat storage of the north wall is mainly concentrated in the small thickness of superficial layer. The added wall thickness cannot accumulate heat masses in the daytime and has no contribution to the exothermic effect inside the CSG during the night. The demerits are the increase of wall thickness causes the waste of manpower and material resources.

Effect of the north wall layered configuration

Previously, the CSG constructions were mostly done by building a single earth or brick wall. Several researchers (Berroug *et al*. [24], Wang *et al*. [25], and Wu and Lei [26]) have claimed that the north wall could append insulation layer as a thermal barrier to reduce the energy loss to outside environment. The thermal insulation layer of the compound wall has been investigated in the present research. Three CSG model with different layer of north wall configuration are compared and discussed. The three models were constructed with the layer walls of inner and outer Styrofoam and brick wall without Styrofoam, respectively.

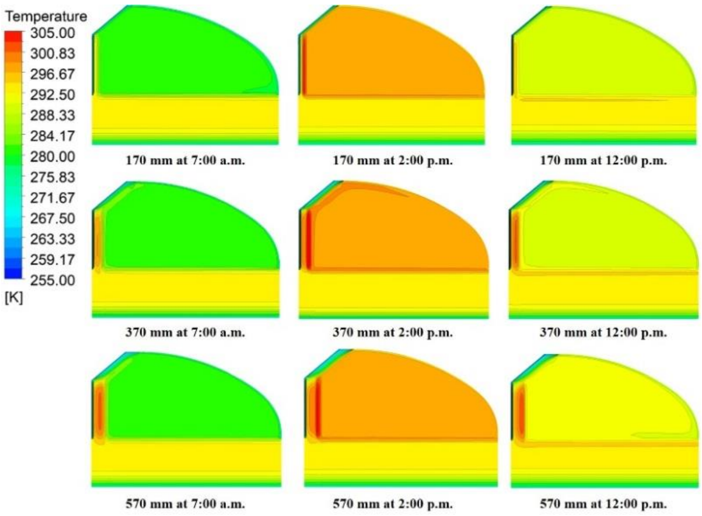

Figure 5. Effect of north wall thickness on the temperature distributions of different instants of time

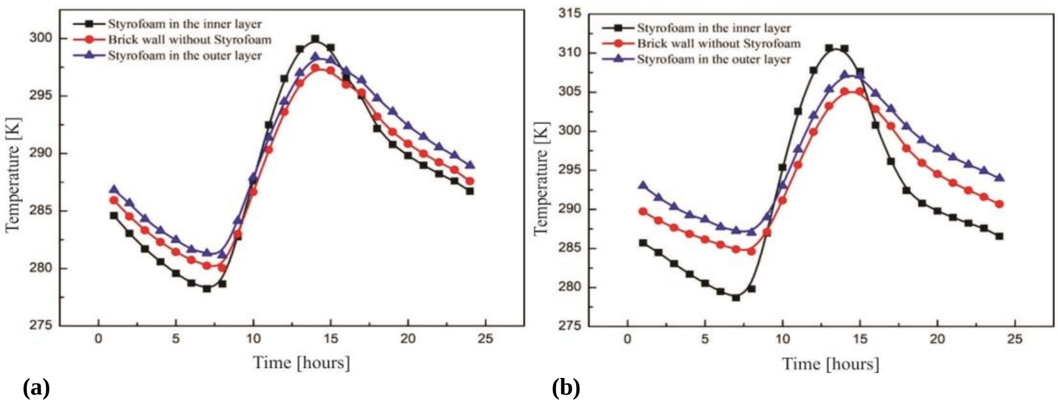

Figure 6. Effect of north wall layered configuration on the internal air temperature (a) and north wall temperature (b)

The Styrofoam layer served as the insulation in the CSG, and the effects are depicted in the gas temperature variations, fig. 6. When the insulation layer is constructed inside of the north wall, the internal gas temperature is highest in the daytime. However, it exhibits a sharp drop in the night. Although the insulation layer avoids heat loss from the north wall to the external environment, in the meantime, it blocks the thermal storage of the wall body. When the insulation layer is constructed outside, the microclimate in the CSG is dramatically improved in comparison to the brick north wall without Styrofoam. In other words, the thermo-stability of the layered wall with insulation outside is much better than the single brick wall. Furthermore, the surface temperature variations of north wall are described in fig. 6(b). From this figure, it is apparent that the layered north wall is not always better than the single brick wall. For instance, it is inappropriate to conduct the insulation layer inside. Even though it builds a high-level thermal environment in the daytime, the north wall loses the heat-retaining capacity in the night. So the thermo-instability is harmful to the winter crop growth. If the thermal insulation is placed in the outer layer, the situation will be greatly improved. In the daytime, the outer insulation layer can reduce unnecessary energy consumption in the thermal storage process to increase the indoor temperature. Moreover, the insulation layer is equipped to promote the positive heat release to the internal environment in the night. The layered north wall in the CSG can significantly enhance the thermal storage capacity as long as the insulation layer is in the proper position.

The temperature distributions on the middle sections in the CSG are shown in fig. 7. Without thermal insulation, the heat transmission of the single brick wall is homogeneous. The solar energy is absorbed in the CSG in the daytime and is dissipated immediately through the enclosures including the north wall. Therefore, the single brick north wall without Styrofoam layer cannot establish a qualified internal thermal environment at night because of the poor heat storage capacity. When a thermal barrier is installed in the inner layer of the north wall, the heat storage of the wall body is directly destroyed. Consequently, the high-temperature environment inside the CSG rapidly drops after sunset. By contrast, the effective way is to install a Styrofoam barrier in the outer layer of the north wall, which can reduce the energy loss during the day and increase the heat preservation at night.

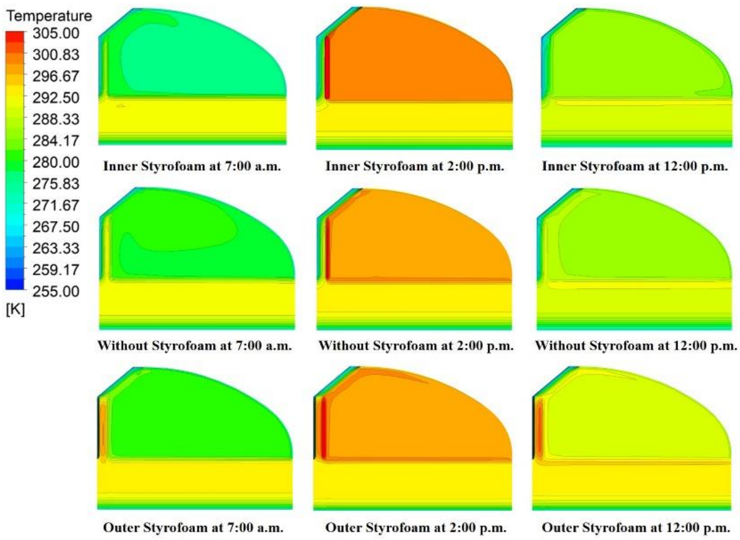

Figure 7. Effect of north wall layered configuration on the temperature distributions of different instants of time

Effect of the north wall material property

Several researchers (Wang *et al*. [3] and Zhang *et al*. [23]) have demonstrated that the material thermal property of the single brick north wall masonry has a crucial influence on the internal microclimate of the traditional greenhouse. Nevertheless, the selection strategy for thermal materials is not entirely applicable to the CSG. Figure 8(a) shows the gas temperature variations of three different north wall materials of clay brick, porous brick, and coal dust brick. The temperature distributions and variation tendencies of three distinct brick layers throughout one day are exactly alike. This suggests that the physical property of the inner brick layer has a small influence on the thermal environment of CSG. The outer insulation layer of the north wall plays a key role in the heat store-release process of CSG, greatly weakening the contribution of the traditional brick layer. The north wall and the soil are the most important thermal enclosures for solar greenhouses. Therefore, the effect of north wall material property on the thermal environment in CSG should be investigated further. Figure 8(b) exhibits the surface temperature variations of north wall. The surface distributions of the three different wall materials are similar, suggesting that the brick layer of north wall is insufficient to dominate the heat-stored and heat-rejected capabilities. The thermal insulation in the outer layer of the north wall plays a vital role in the thermal maintenance for winter crop. The CSG significantly relaxes the high requirements for the thermal properties of the north wall.

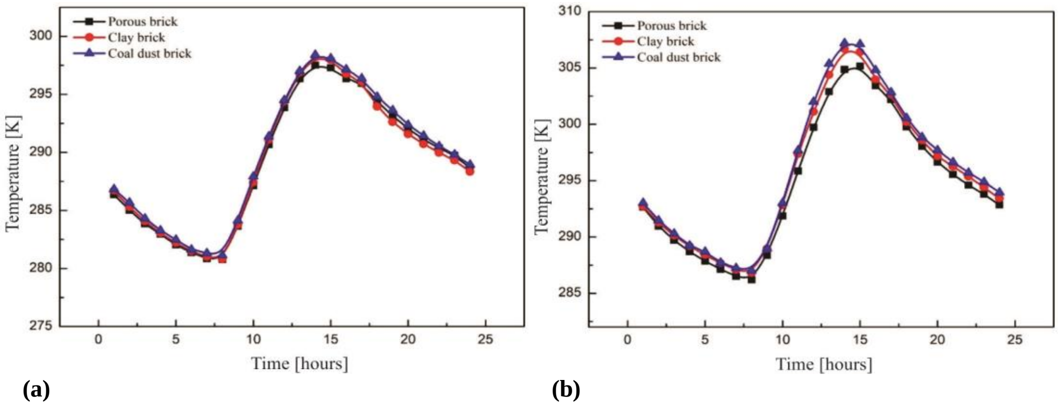

Figure 8. Effect of north wall material property on the internal air temperature (a) and north wall temperature (b)

Figure 9 describes the global temperature distributions of the three different north wall materials. The CSG north walls made of clay brick and coal dust brick generate the similar indoor temperature distributions, which are slightly different from that the porous brick north wall. The thermal conductivity of the clay brick (*i. e.* 0.50 W/mK) and the coal dust brick (*i. e.* 0.51 W/mK) is almost the same.

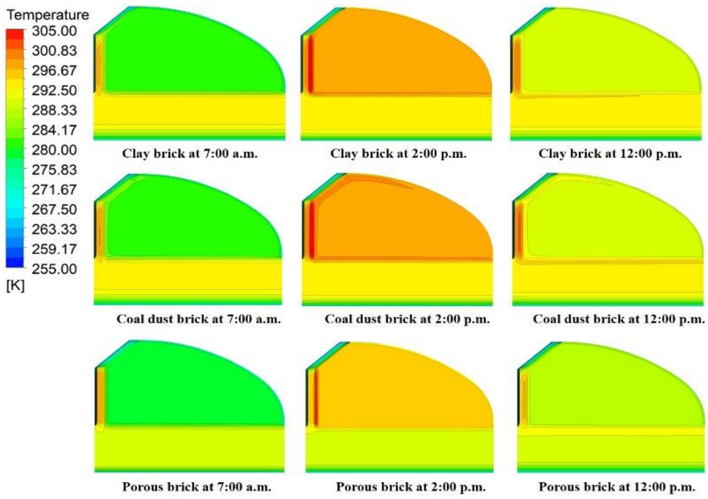

Figure 9. Effect of north wall layered configuration on the temperature distributions of different instants of time

However, the same property for the porous brick (*i. e.* 0.58 W/mK) is slightly higher. Therefore, the heat accumulation and emission of the porous brick north wall are faster. The specific heat capacity of the three north wall is not the same. The clay brick is the smallest (*i. e.* 989.3 J/kg°C), the coal dust brick is the second smallest (*i. e.* 1051.1 J/kg°C), and the porous brick is the largest (*i. e.* 1062.3 J/kg°C). Nevertheless, the differences of heat storage capacity between different north walls are insignificant on account of the same thermal insulation in the outer layer. The results indicate that the specific heat capacity has relatively less effect on the thermal storage and release of the north wall in CSG than the thermal conductivity. As a consequence, the prospective CSG could phase out the traditional solar greenhouse made of single brick north wall owing to its low cost and high efficiency.

Conclusion

A numerical investigation of the CSG thermal performance has been carried out in the present research. The predicted results agree well with the validated experimental measurements. The thermal performances are described hourly in the visualized expressions. Depending on the obtained results, there is a limit to the improvement of thermal performance with the increase of north wall thickness. The heat storage of the north wall is mainly concentrated in the superficial layer and the added wall thickness could bring about wasted resources. The thermal performance of layered north wall with a Styrofoam barrier in the outer layer is much better than that of the single brick wall. The heat insulation layer contributes to the thermal accumulation and preservation. The inner brick layer has little effect on the thermal performance of the north wall while the outer insulation layer plays a key role in the heat store-release process. The CSG significantly reduces the requirements for the thermal properties of the north wall.

Acknowledgement

The authors are especially grateful to Neven Duić, Marko Ban and Milan Vujanović from SDEWES for their invaluable comments and suggestions that helped to significantly improve this research. This work was supported by the National Post Expert Project of Staple Vegetable Technology (Grant No. CARS-23-C01).

References

[1] Hassanain, A. A., *et al*., Effect of Solar Storage Wall on the Passive Solar Heating Constructions, *Energy Build., 43* (2011), 2-3, pp. 737-747
[2] Dragicevic S. M., Determining the Optimum Orientation of a Greenhouse on the Basis of the Total Solar Radiation Availability, *Thermal Science, 15* (2011), 1, pp. 215-221
[3] Wang, J., *et al*., Analysis of Heat Transfer Properties of Hollow Block Wall Filled by Different Materials in Solar Greenhouse, *Engineering in Agriculture, Environment and Food, 10* (2017), 1, pp. 31-38
[4] Zhang, G., *et al*., Computational Fluid Dynamics (CFD) Research and Application in Agricultural and Biological Engineering, *Comput. Electron. Agric., 149* (2018), June, pp. 1-2
[5] Tong, G., *et al*., Passive Solar Energy Utilization: A Review of Cross-section Building Parameter Selection for Chinese Solar Greenhouses, *Renew. Sust. Energ. Rev., 26* (2013), Oct., pp. 540-548
[6] Chen, C, *et al*., Thermal Performance of an Active-passive Ventilation Wall with Phase Change Material in Solar Greenhouses, *Appl. Energy, 216* (2018), Apr., pp. 602-612
[7] Bartzanas, T., *et al*., Effect of Vent Arrangement on Windward Ventilation of a Tunnel Greenhouse, *Biosyst. Eng., 88* (2004), 4, pp. 479-490
[8] Boulard, T., Wang, S., Experimental and Numerical Studies on the Heterogeneity of Crop Transpiration in a Plastic Tunnel, *Compu.t Electron. Ag.r, 34* (2002), 1-3, pp. 173-190

[9] Bournet, P. E., *et al*, Numerical Prediction of the Effect of Vent Arrangements on the Ventilation and Energy Transfer in a Multi-span Glasshouse Using a Bi-band Radiation Model, *Biosyst. Eng., 98* (2007), 2, pp. 224-234

[10] Fath, H. E. S., Abdelrahman, K., Micro-climatic Environmental Conditions inside a Greenhouse with a Built-in Solar Distillation System, *Desalination, 171* (2005), 3, pp. 267-287

[11] Kacira, M., *et al*., A CFD Evaluation of Naturally Ventilated, Multi-span, Sawtooth Greenhouses, *Transactions of the American Society of Agricultural Engineers, 41,* (1998), 3, pp. 833-836

[12] Mistriotis, A., Briassoulis, D., Numerical Estimation of the Internal and External Aerodynamic Coefficients of a Tunnel Greenhouse Structure with Openings, *Comput. Electron. Agr., 34* (2002), pp. 191-205

[13] Molina-Aiz, F. D., *et al*., Measurement and Simulation of Climate inside Almería-type Greenhouses Using Computational Fluid Dynamics, *Agr. Forest Meteorol., 125* (2004), 1-2, pp. 33-51

[14] Vanthoor, B. H. E., *et al*., A Methodology for Model-based Greenhouse Design: Part 5, Greenhouse Design Optimisation for Southern-Spanish and Dutch Conditions, *Biosyst. Eng., 111* (2012), 4, pp. 350-368

[15] Ajabshirchi, Y., *et al*., Solar Energy Conservation in Greenhouse: Thermal Analysis and Experimental Validation, *Renew. Energ., 96* (2016), Part A, pp. 509-519

[16] Öztürk, H. H., Experimental Evaluation of Energy and Energy Efficiency of a Seasonal Latent Heat Storage System for Greenhouse Heating, *Energy Conversion and Management, 46* (2005), 9-10, pp. 1523-1542

[17] Boulard, T., *et al*., Modelling of Micrometeorology, Canopy Transpiration and Photosynthesis in a Closed Greenhouse Using Computational Fluid Dynamics, *Biosyst. Eng., 158* (2017), June, pp. 110-133

[18] Ling, H., *et al*., Indicators Evaluating Thermal Inertia Performance of Envelops with Phase Change Material, *Energ. Buildings, 122* (2016), June, pp. 175-184

[19] Tong, G., *et al*., Numerical Modelling of Temperature Variations in a Chinese Solar Greenhouse, *Comput. Electron. Agr., 68* (2009), 1, pp. 129-139

[20] Zhou, N., *et al*., A Study on Thermal Calculation Method for a Plastic Greenhouse with Solar Energy Storage and Heating, *Sol. Energy, 142* (2017), Jan., pp. 39-48

[21] Ren, J., *et al*., Study on the Hygrothermal Properties of a Chinese Solar Greenhouse with a Straw Block North Wall, *Energ. Buildings, 193* (2019), June, pp. 127-138

[22] Wang, S., *et al*., Numerical Study on Dynamic Thermal Characteristics and Optimum Configuration of Internal Walls for Intermittently Heated Rooms with Different Heating Durations, *Appl. Therm. Eng., 155* (2019), June, pp. 437-448

[23] Zhang, J., *et al*., Study on Heat Transfer Characteristics of Straw Block Wall in Solar Greenhouse, *Energ. Buildings, 139* (2017), Mar., pp. 91-100

[24] Berroug, F., *et al*., Thermal Performance of a Greenhouse with a Phase Change Material North Wall, *Energ. Buildings, 43* (2011), 11, pp. 3027-3035

[25] Wang, *et al*., Simulation and Optimization of Solar Greenhouses in Northern Jiangsu Province of China, *Energ. Buildings, 78* (2014), Aug., pp. 143-152

[26] Wu, T., Lei, C., A Review of Research and Development on Water Wall for Building Applications, *Energ. Buildings, 112* (2016), Jan., pp. 198-208

Paper submitted: February 2, 2020
Paper revised: April 15, 2020
Paper accepted: May 2, 2020